



# Photocatalytic activities of novel $\text{SrTiO}_3$ – $\text{BiOBr}$ heterojunction catalysts towards the degradation of reactive dyes

Thamaraiselvi Kanagaraj, Sivakumar Thiripuranthagan\*

Department of Applied Science and Technology, A.C. Tech., Anna University, Chennai-25, Tamilnadu, India

## ARTICLE INFO

### Article history:

Received 30 November 2016

Received in revised form 18 January 2017

Accepted 31 January 2017

Available online 8 February 2017

### Keywords:

$\text{SrTiO}_3$  nanocubes

Mesoporous  $\text{BiOBr}$

Heterojunction

Visible light activity

Photocatalysis

## ABSTRACT

$\text{SrTiO}_3$  nanocube and three dimensional, mesoporous  $\text{BiOBr}$  catalysts were synthesized by sol-gel and precipitation methods respectively. Various weight percentages of  $\text{SrTiO}_3$ - $\text{BiOBr}$  heterojunction composite catalysts ( $x\% \text{SrTiO}_3\text{-BiOBr}$  where  $x = 5, 10, 30, 50 \& 70$  percentage of  $\text{SrTiO}_3$ ) were synthesized by impregnation method. All the synthesized catalysts were characterized by various instrumental techniques. The results of PL and EIS indicate that the heterojunction catalyst, 10%  $\text{SrTiO}_3$ - $\text{BiOBr}$  (10-ST/BB), has the lowest recombination rate of  $e^- - h^+$  pairs and the lowest electron transfer resistance respectively. Photocatalytic activities of the synthesized catalysts were tested towards the degradation of carcinogenic reactive dyes such as reactive blue 198, reactive black 5 and reactive yellow 145 in presence of visible and solar irradiations. Among the catalysts 10-ST/BB resulted in the highest photocatalytic activity towards the degradation of all the three dyes. Kinetics studies on degradation indicated that it followed pseudo first order. The efficiency of dye degradation was found to be better in the presence of solar light than under visible light degradation due to  $\simeq 4\%$  UV light in solar irradiation. TOC, HPLC and COD studies confirm that the dyes are mineralized into some organic salts such as acetates, formates, etc.,  $\text{CO}_2$ , water and salts.

© 2017 Elsevier B.V. All rights reserved.

## 1. Introduction

Dyes from dyeing, textile, tanning and paint industries are the major pollutants of the environment. More than 10,000 different dyes are produced annually and out of that 1000 tons of dyes are released into rivers and other water bodies [1–5]. As most of these dyes are non biodegradable, they pose severe threat to all living organisms carrying respiratory problem, asthma, dermatitis, mutagenicity, cancer, etc. [6–10]. The strong colour of reactive dyes is due to the presence of chromophores such as azo, anthraquinone and phthalocyanine groups. Among the reactive dyes the azo dyes are widely used. Hence numbers of attempts have been made in the past to degrade the toxic reactive azo dyes [11–13]. Since the conventional treatment techniques such as adsorption, flocculation, ozonation, membrane filtration, etc have their own advantages and limitations, a greener technique such as advanced oxidation process (AOP) is sought [14,15]. Among the different AOPs, photocatalytic degradation using semiconductor oxides has attracted many researchers. In advanced oxidation processes, mostly titania is used as the photocatalyst due to its high chemical stability and

oxidising power but due to its the large bandgap, the charge carriers ( $e^- - h^+$ ) recombine and limits its activity only in UV region not in visible region [16,17]. In order to reduce the bandgap and prevent recombination several strategies have been carried out and reported [18–20]. One of our authors also reported several modifications such as elemental doping, impregnation, etc [21–26].

Strontium titanate a cubic perovskite is very similar to titania and is used for degradation purpose but only in the UV region. Due to the intrinsic wide bandgap of 3.22 eV for strontium titanate it can be utilized only in the UV region and hence rapid recombination of electron and hole pair occurs which greatly reduces the quantum efficiency. Hence there is a great need to develop means and ways to widen the light absorption region and prevent recombination. Many noble metal and metal oxides were also doped into or impregnated over  $\text{SrTiO}_3$  [27–30]. Besides noble metals, semi conductors also have been impregnated to improve visible activity. In this context, bismuth oxyhalides with tetragonal maitlockite structure also have been tried for photocatalytic applications.  $\text{BiOBr}$  in general is more active due to its stability and suitable band gap between O 2p and Bi 6s. It is one of the best visible active semiconductor that has been employed for photocatalytic degradations [31–34].  $\text{BiOBr}$  with different morphologies such as mesoporous hierarchical spheres, nanoplates, nanoparticles, nanobelts synthesized by different methods such as hydro or solvothermal, electrospinning,

\* Corresponding author.

E-mail address: [tssivakumar@yahoo.com](mailto:tssivakumar@yahoo.com) (S. Thiripuranthagan).

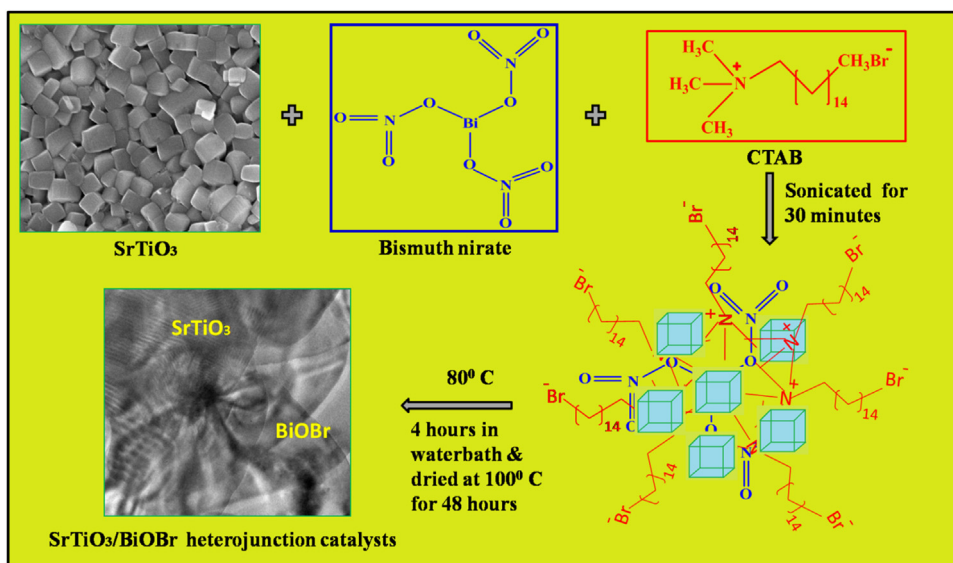


Fig. 1. Scheme showing the synthesis of SrTiO<sub>3</sub>/BiOBr composite catalysts.

etc. have been reported [35–38]. In BiOBr, [Bi<sub>2</sub>O<sub>2</sub>]<sup>2+</sup> layers are interleaved with double bromide layers. This unique structure combined with strong electrostatic field contribute to the effective separation and transfer of electron and hole pairs. To improve the catalytic activity of BiOBr, it has been combined or heterojunctioned with different materials [39,40]. On the other hand, SrTiO<sub>3</sub> is a cubic perovskite with high lattice order and low electron hole pair recombination but a wide bandgap limits its application in the visible range [41,42]. Fabricating a heterojunction between SrTiO<sub>3</sub> and BiOBr with suitable bandgap and band position is an alternative way to get rid of the twin issues of SrTiO<sub>3</sub>. Hence it was planned to prepare heterojunction catalysts combining the highly stable crystalline SrTiO<sub>3</sub> with visible active BiOBr and evaluate the catalytic activity in both visible and sunlight irradiations towards the degradation of three different reactive dyes namely reactive blue 198, reactive black 5 and reactive yellow 145. The results show that among the different heterojunction catalysts, 10-ST/BB catalyst showed the highest catalytic activity towards the degradation of all the three reactive dyes.

## 2. Experimental section

### 2.1. Materials

SrCl<sub>2</sub>·6H<sub>2</sub>O ( $\geq 99\%$  purity), Ti{OCH(CH<sub>3</sub>)<sub>2</sub>}<sub>4</sub> (97% purity), glacial CH<sub>3</sub>COOH ( $\geq 99.7\%$  purity) and Bi(NO<sub>3</sub>)<sub>2</sub>·5H<sub>2</sub>O ( $\geq 98\%$  purity) were purchased from Sigma- Aldrich, India. CTAB (99% purity) was purchased from SRL Chemicals, India. Reactive blue 198 (98% purity) was procured from R.A. dyestuffs (INDIA) Pvt.ltd. India, whereas the other two dyes namely Reactive Yellow 145 (98% purity) and Reactive Black 5 (95% purity) dyes were obtained from Colourise Industries., India. All the chemicals were used without any further purification.

### 2.2. Synthesis of catalysts

#### 2.2.1. Synthesis of SrTiO<sub>3</sub>

Strontium titanate was synthesized by sol-gel method. 11.84 ml of titanium isopropoxide was dissolved in 20 ml of acetic acid and 20 ml water was added to it and stirred till clear transparent solution was obtained. 10.664 g of strontium chloride dissolved in 20 ml of water and 4 M citric acid was added to the above solution and pH

was adjusted to 1.5. The solution was stirred whole night (15 h) and heated in waterbath at 65 °C for 4 h. The viscous sol obtained was again heated at 110 °C for 12 h. A brown mass formed was dried at 180 °C for 12 h and heated at 400 °C for 12 h till it changed into white powder. The product was finally calcined at 650 °C for another 12 h [43].

#### 2.2.2. Synthesis of BiOBr

Bismuth oxybromide was synthesized by precipitation method. Aqueous solution containing 5.39 g of Bi(NO<sub>3</sub>)<sub>2</sub>·5H<sub>2</sub>O was taken and the pH was adjusted to neutral. 50 ml of 0.008 M cetyl trimethyl ammonium bromide (CTAB) was taken and bismuth nitrate solution was added dropwise and stirred. Then the solution was sonicated for 15 min and kept in waterbath for 3 h at 80 °C. The precipitate obtained was washed with water and ethanol several times and dried at 100 °C for 48 h [44].

#### 2.2.3. Synthesis of SrTiO<sub>3</sub>/BiOBr heterojunction catalysts

Scheme of the synthesis of SrTiO<sub>3</sub>/BiOBr composite catalyst by impregnation method is shown in Fig. 1. Stoichiometric amounts of bismuth nitrate and CTAB were dissolved in water. Various weight percentages (5, 10, 30, 50 & 70) of as synthesized SrTiO<sub>3</sub> were added to the above solution and sonicated for 30 min. White suspension obtained was kept in waterbath at 80 °C for 4 h, centrifuged, washed with water and ethanol and dried at 100 °C for 48 h. The corresponding composites obtained were named as 5-ST/BB, 10-ST/BB, 30-ST/BB, 50-ST/BB and 70-ST/BB respectively.

### 2.3. Characterization

X-ray diffraction (XRD) patterns of synthesized catalysts were recorded on PANalytical- X'Pert PRO using Cu K $\alpha$  (Lambda = 0.154 nm) radiation to confirm the phase formation. The average crystallite size of the catalysts was calculated using the Scherrer's formula ( $D = K\lambda/\beta \cos \theta$ ). UV- diffuse reflectance spectra of synthesized photocatalysts were recorded on Jasco (V-650) UV-vis spectrophotometer using BaSO<sub>4</sub> as a reference in the wavelength range of 200–800 nm to determine their bandgap values. X-ray photoelectron spectral measurements were done to determine the elements present in the catalyst on an ECALAB MKIV XPS system. Nitrogen adsorption-desorption isotherms were recorded by using Quantachrome Asiqwine Brunauer–Emmett–Teller (BET)

**Table 1**

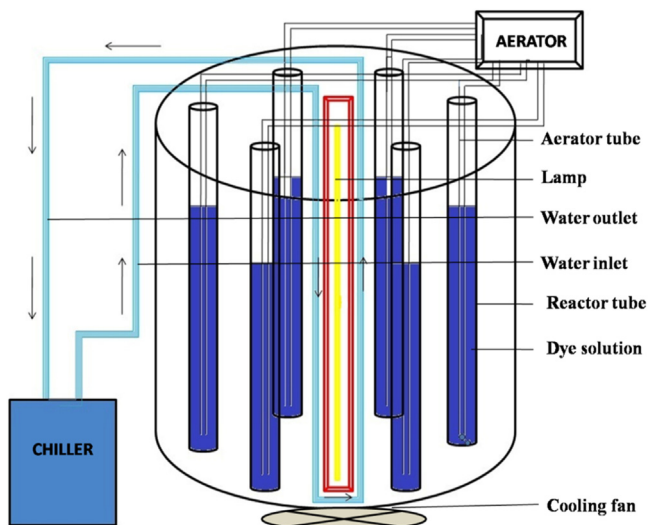
Physicochemical properties of three reactive dyes.

CI Name	Structure	Molecular Weight (g)	$\lambda_{\max}$ (nm)	No. of azo groups
Reactive blue 198		1682.6	625	Diazo
Reactive black 5		991.82	600	Diazo
Reactive yellow 145		1026.25	418	Monoazo

surface area analyzer. The surface area of the catalysts were determined at 77 K temperature after degassing the catalysts at 100 °C under vacuum. High Resolution Scanning Electron Micrographs were recorded to know the morphology of the catalysts by Hitachi UHR SU8000 SEM instrument. Elemental mapping and energy dispersive spectra were also performed for the most active catalyst to confirm the presence of elements in the catalyst. Particle size, surface morphology and selected area electron diffraction of the best catalyst was taken by using high resolution transmission electron microscope (HITACHI HT7700). Photoluminescence spectra were obtained by Horiba LabRAM HR micro PL instrument (excitation wavelength is 325 nm with He-Cd laser) to know the effect of electron hole pair recombination in the catalysts. Electrochemical impedance spectra were recorded by VMP-3 Bio-Logic Electrochemical Work Station equipped with three electrodes namely working electrode, a standard Ag/AgCl in saturated KCl as reference electrode and a platinum wire as counter electrode. The working electrode was coated with the mixture of the catalyst and the binder n-butyl carbitol (9:1 weight ratio). The slurry obtained was brush coated on carbon sheets, dried and sintered at 400 °C for one hour to maintain uniform thickness. Then the electrochemical impedance measurements were made at inert gas (N<sub>2</sub>) atmosphere with an open circuit potential.

#### 2.4. Photocatalytic evaluation studies

The photocatalytic activities of all the synthesized catalysts were evaluated towards the degradation of three reactive azo dyes such as reactive blue 198, reactive black 5 and reactive yellow 145. Structure and  $\lambda_{\max}$  of the dyes are given in Table 1. The photocatalytic degradation of three dyes was carried out in an immersion type visible reactor (Heber Scientific Company Ltd., Chennai) equipped with 500 W tungsten lamp (420 nm) with water circulation to avoid thermal decolorization. The schematic representation of reactor is shown in Fig. 2. 100 ml (50 ppm) of dye

**Fig. 2.** Schematic diagram of visible reactor for dye degradation.

solutions along with 0.1 g of different catalysts were taken in six quartz tubes for decolorization reaction. Dark reaction was carried out for the first 30 min to attain adsorption-desorption equilibrium. Photolysis was also performed without the catalysts. The samples were collected at regular intervals (15 min) and analyzed by UV-vis Spectrophotometer (HITACHI U-2000). The absorbance values were measured and the percentage decolorization was calculated by the following equation:

$$\text{Percentagedecolourization} = [100 - (C/C_0 \times 100)] \quad (1)$$

Where, C<sub>0</sub> and C are the concentration of dye at initial and at respective time.

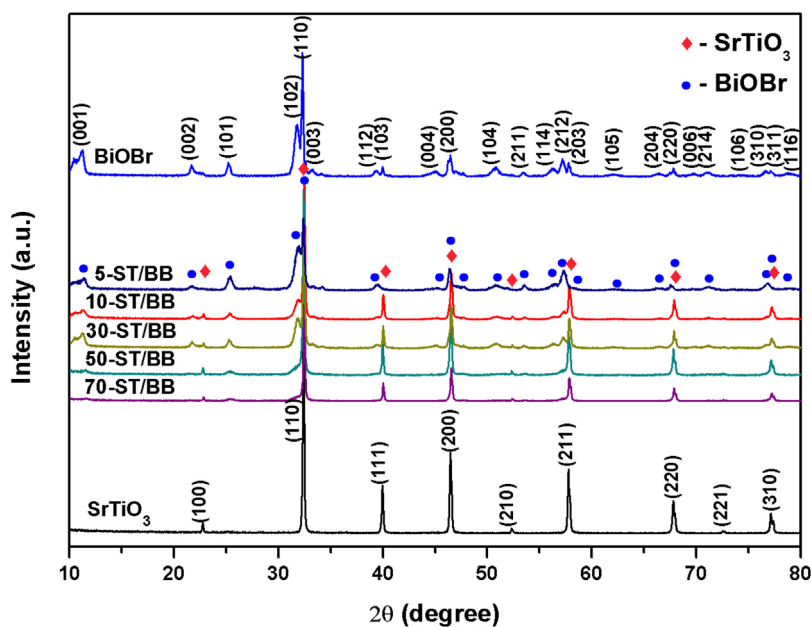


Fig. 3. XRD patterns of bare  $\text{SrTiO}_3$ ,  $\text{BiOBr}$  and composite catalysts.

### 2.5. Photodecolourization under sunlight

Photodecolourization under solar irradiation was performed in the month of April between 11:00 A.M. and 12:00 P.M. in the open terrace for the most active catalyst (discussed later). The solar light intensity was measured by luxmeter and was found to be  $9.49 \times 10^4$  lx. 100 ml of 50 ppm of each dye with 100 mg of different catalysts were taken in a glass beaker for decolourization reaction and an aerator was used for incessant dispersion of catalyst particles in the dye solution. Sampling has been done for every 5 min and analyzed as discussed before.

### 2.6. Photodegradation studies of reactive dyes by using HPLC

All the three reactive dyes have very big molecular structure and during the degradation process it breaks and forms intermediates. To find the concentration of intermediates and the degradation percentage, high performance liquid chromatographic analysis (Agilent 2160 infinity HPLC instrument) was performed for samples collected at different intervals of time after filtering through the  $0.22 \mu\text{m}$  nylon syringe filter. ZORBAX SB-C18 ( $4.6 \times 250$  mm,  $5 \mu\text{m}$ ) column was used and column pressure was maintained from 57–63 bar. A mixture of methanol and water (30:70) was used ( $1 \text{ ml}/\text{min}$ ) as mobile phase.  $1 \mu\text{l}$  sample was injected and detected by UV detector at 250 nm.

## 3. Result and discussion

### 3.1. Characterization of as synthesized

#### 3.1.1. Structural properties

XRD patterns of  $\text{SrTiO}_3$ ,  $\text{BiOBr}$  and ST/BB heterojunction catalysts are shown in Fig. 3. Appearance of sharp peaks confirmed the highly crystalline nature of strontium titanate. The peaks present at  $2\theta$  values  $22.75^\circ$ ,  $32.39^\circ$ ,  $39.95^\circ$ ,  $46.47^\circ$ ,  $52.34^\circ$ ,  $57.78^\circ$ ,  $67.83^\circ$ ,  $72.57^\circ$  and  $77.19^\circ$  were indexed as the  $100$ ,  $110$ ,  $111$ ,  $200$ ,  $210$ ,  $211$ ,  $220$ ,  $221$ , and  $310$  planes respectively of  $\text{SrTiO}_3$  with cubic phase ( $\text{Pm}3\text{m}$ ) (JCPDS card No. 73-0661) [45].  $\text{BiOBr}$  diffraction pattern shows the peaks at  $10.90^\circ$ ,  $21.92^\circ$ ,  $25.15^\circ$ ,  $31.69^\circ$ ,  $32.21^\circ$ ,  $33.12^\circ$ ,  $39.38^\circ$ ,  $40.43^\circ$ ,  $44.69^\circ$ ,  $46.20^\circ$ ,  $50.67^\circ$ ,  $53.37^\circ$ ,  $56.14^\circ$ ,  $57.11^\circ$ ,  $58.02^\circ$ ,

Table 2

Surface area, pore volume, particle size and bandgap values of bare  $\text{BiOBr}$ ,  $\text{SrTiO}_3$  and ST/BB heterojunction composite catalysts.

Catalyst	Surface Area ( $\text{m}^2/\text{g}$ )	Particle size (nm)	Bandgap (eV)
$\text{SrTiO}_3$	24.6	8.6	3.22
5-ST/BB	7.3	58.1	2.87
10-ST/BB	11.9	62.3	2.80
30-ST/BB	8.3	68.4	2.87
50-ST/BB	6.7	43.5	2.92
70-ST/BB	9.4	42.0	2.92
$\text{BiOBr}$	5.0	69.5	2.86

$61.90^\circ$ ,  $66.21^\circ$ ,  $67.40^\circ$ ,  $69.54^\circ$ ,  $71.00^\circ$ ,  $74.19^\circ$ ,  $76.69^\circ$ ,  $77.75^\circ$  and  $78.72^\circ$  for the corresponding planes of  $001$ ,  $002$ ,  $101$ ,  $102$ ,  $110$ ,  $003$ ,  $112$ ,  $103$ ,  $004$ ,  $200$ ,  $104$ ,  $211$ ,  $114$ ,  $212$ ,  $203$ ,  $105$ ,  $204$ ,  $220$ ,  $006$ ,  $214$ ,  $106$ ,  $310$ ,  $311$  and  $116$  of tetragonal ( $p4/nmm$ )  $\text{BiOBr}$  (JCPDS card No. 09-0393) [46]. ST/BB heterojunction catalysts had both  $\text{SrTiO}_3$  and  $\text{BiOBr}$  signatures.  $110$  plane of  $\text{SrTiO}_3$  ( $32.39^\circ$ ) and  $\text{BiOBr}$  ( $32.31^\circ$ ) were closer to each other and showed almost a single peak in heterojunction catalysts. But diminutive shift happened from  $32.31^\circ$  to  $32.39^\circ$  when the percentage weight of strontium titanate increased. The average crystallite size of all the catalysts was calculated by Scherrer's formula.

$$D = \frac{K\lambda}{\beta} \cos\theta \quad (2)$$

where  $D$  is the average crystal size,  $K$  the constant (0.89),  $\lambda$  the wavelength of the  $\text{Cu K}\alpha$  radiation (1.54),  $\beta$  the full width at half maximum for the  $(101)$  plane, and  $\theta$  is the diffraction angle. The particle size of all the catalysts is listed in Table 2.

Fig. 4a shows the XPS survey spectrum of the most active 10-ST/BB. The peaks appeared in the spectrum denote the electronic and oxidation states originated from the emission of photoelectrons. The binding energy peaks appeared confirms the presence of dominant elements Sr (3p and 3d), Ti (2p and 3p), Bi (4p, 4d, 4f and 5d), Br (3d) and O (1s) in 10-ST/BB heterojunction catalyst [47,48]. The petite variations in the binding energies of the elements were raised by the ejection of photoelectrons from various electronic environments and hence peak positions were chemical shifted [49]. The individual XPS peaks of Ti 2p (+4 oxidation state) observed

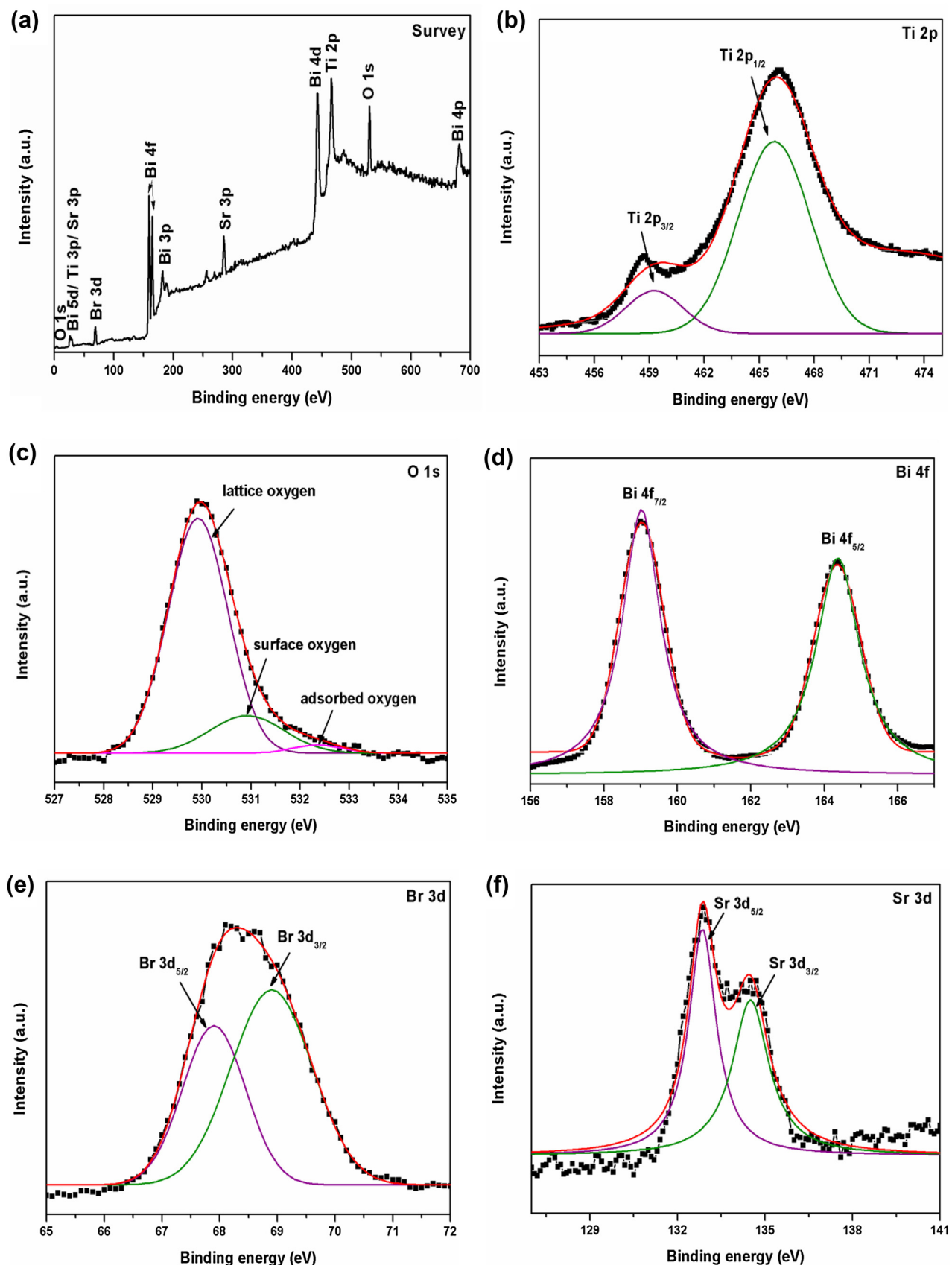


**Fig. 4.** XPS spectra for 10-ST/BB heterojunction catalyst (a) Overall spectrum and (b–f) individual elements spectra.

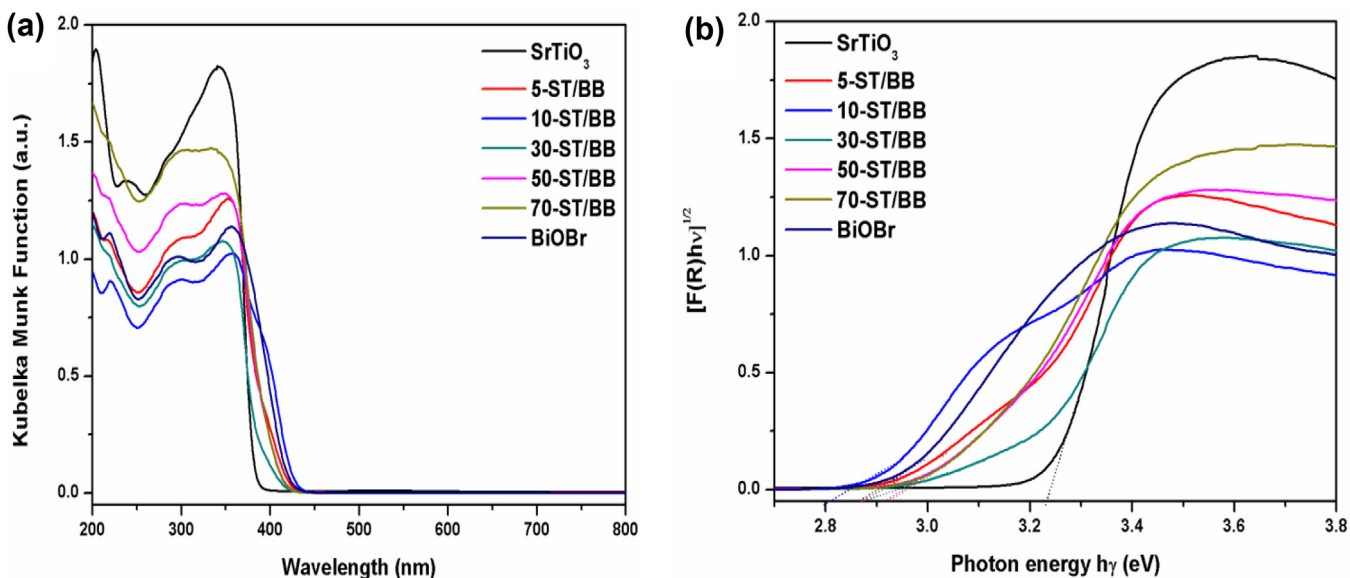


Fig. 5. UV-vis absorption (DRS) spectra of bare and composite catalysts in terms of (a) Kubelka Munk function and (b) photon energy.

at 459.2 eV and 465.82 eV binding energies denote the doublet Ti 2p<sub>3/2</sub> and Ti 2p<sub>1/2</sub> respectively (Fig. 4b) [50]. The peaks at 529.96 eV, 531.21 eV and 532.5 eV in Fig. 3c were attributed to O 1s. These three peaks indicate the different types of oxygen molecule such as lattice oxygen, surface oxygen and adsorbed oxygen [51]. Spin orbit splitting of Bi 4f (+3 oxidation state) at 158.99 eV and 164.38 eV binding energies describe the 4f<sub>7/2</sub> and 4f<sub>5/2</sub> states (Fig. 4d) [52]. Peaks observed at the binding energies of 67.88 eV and 68.92 eV in Fig. 4e correspond to Br 3d<sub>5/2</sub> and Br 3d<sub>3/2</sub> splitting of 3d orbital of bromide (Br<sup>−</sup>) ion [32]. Fig. 4f explains the splitting of Sr 3d into two peaks at 132.98 eV and 134.79 eV binding energies for respective Sr 3d<sub>5/2</sub> and Sr 3d<sub>3/2</sub> states respectively [53]. According to Koopman's theorem peak splitting in Sr, Ti, Br and Bi happened due to the energy difference between singlet and triplet states of orbitals [54].

### 3.1.2. Optical properties

Optical properties of the as synthesized catalysts are derived from UV diffuse reflectance spectra. Wavelength versus Kubelka Munk function of all the synthesized catalysts show different absorption edges (Fig. 5a). Strontium titanate shows cut off wavelength at 385 nm whereas bare BiOBr and the composite catalysts show the absorption edges in the visible (>400 nm) region. The bandgap energies of the catalysts were calculated from Fig. 5b using modified Tauc, Davis and Mott expression [55–58].

$$[F(R)h\gamma]^{\frac{1}{n}} = A (h\gamma - E_g) \quad (3)$$

Where,  $\alpha$  is the absorption coefficient,  $h$  is the Planck's constant,  $\gamma$  is the vibration frequency,  $E_g$  is bandgap,  $A$  is the proportional constant and  $n$  is the nature of transition. Since both SrTiO<sub>3</sub> and BiOBr had the indirect allowed transition  $n = 2$  was substituted in Eqn. (3) [59,60].

The intercept of linear portion in the plot of photon energy ( $h\gamma$ ) versus  $[F(R)h\gamma]^{\frac{1}{2}}$  gave the bandgap energy of the catalysts directly (Table 1). SrTiO<sub>3</sub> shows the highest bandgap energy. When BiOBr was junctioned with SrTiO<sub>3</sub> it creates the impurity in the energy level of SrTiO<sub>3</sub> and hence modifies the optical properties in visible region. Therefore the composite catalysts showed lower bandgap values than bare SrTiO<sub>3</sub>. Among all the catalysts, 10-ST/BB showed the lowest bandgap value and hence electronic transitions are easily assisted [61].

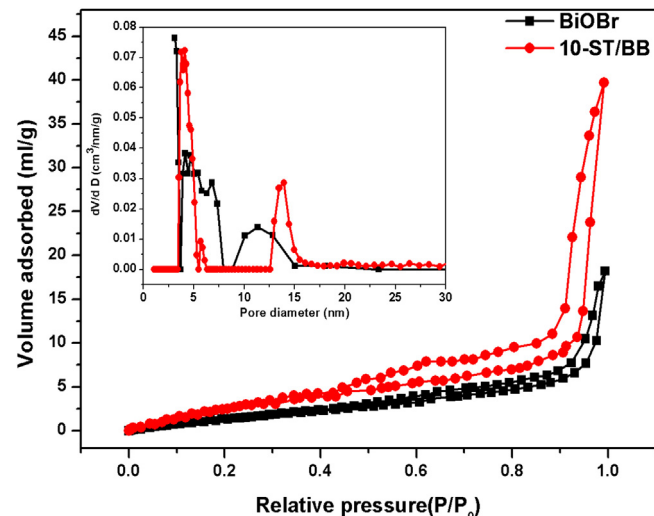
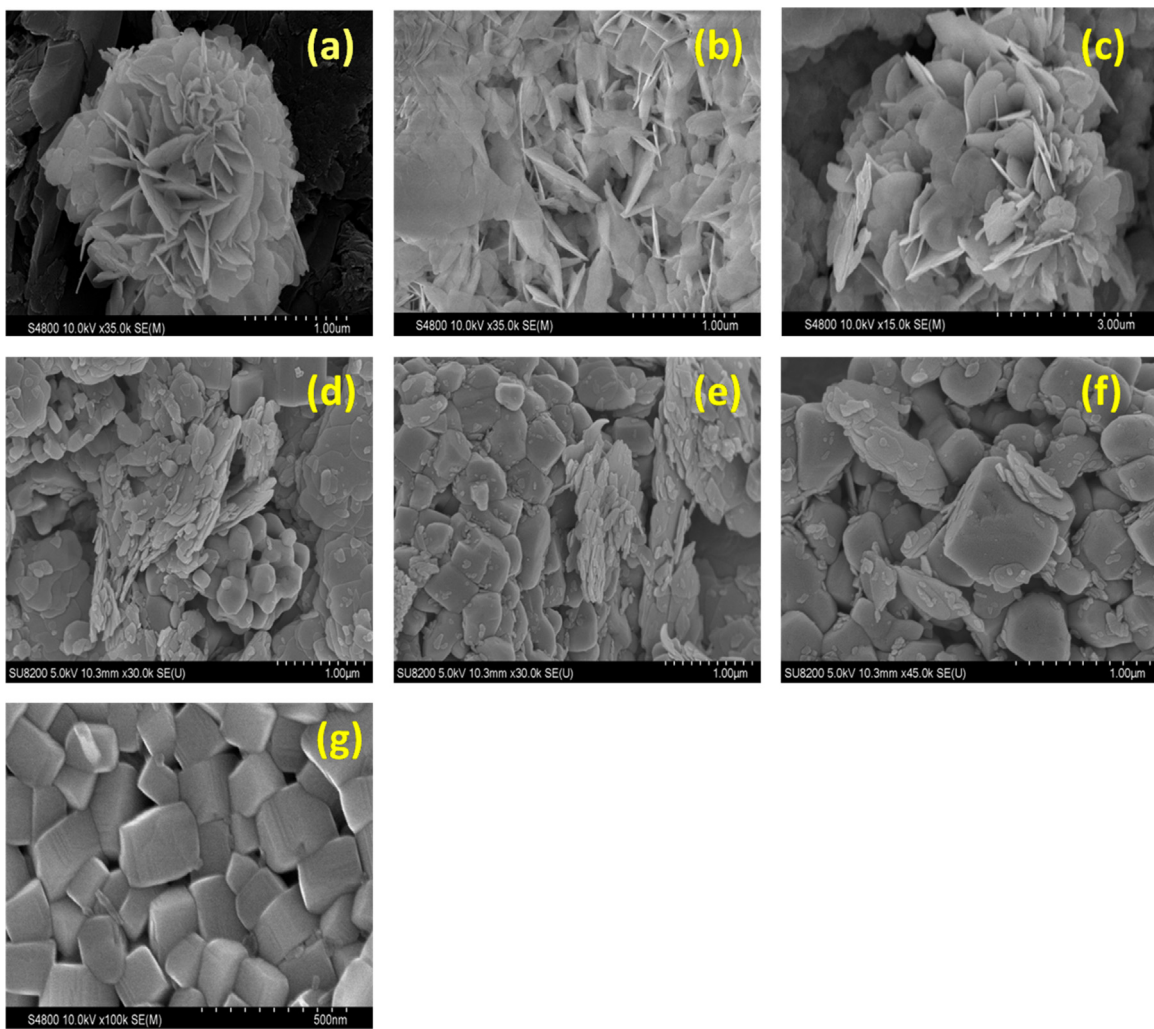


Fig. 6. N<sub>2</sub> adsorption-desorption isotherms of BiOBr and 10-ST/BB catalysts (Inset: Pore size distribution curves).

### 3.1.3. Structural and morphological properties

Fig. 6 illustrates the N<sub>2</sub> adsorption-desorption isotherms of bare BiOBr and the most active 10-ST/BB catalysts. Both BiOBr and 10-ST/BB catalysts exhibit the type IV isotherm with H<sub>3</sub> hysteresis loop indicating the mesoporous nature and wide pore size distribution of the catalysts [62,63]. The inset is pore size distribution plots, which show many peaks between 3 and 15 nm for both BiOBr and 10-ST/BB catalysts. This indicates the mesoporous nature with wide pore size distribution. Average pore diameter of BiOBr and 10-ST/BB as calculated by BJH pore size determination were found to be 9.7 nm and 10.23 nm respectively. Surface area of all the catalysts was determined and given in Table 2. BiOBr possesses very low surface area (5 m<sup>2</sup>/g) whereas strontium titanate had the surface area of 24.6 m<sup>2</sup>/g. As there is no limiting adsorption at high P/P<sub>0</sub> in the isotherm with H<sub>3</sub> hysteresis, the composite may exist either as plate like particles or may have slit shaped pores. Among the heterojunction catalysts 10-ST/BB showed the highest surface area (11.9 m<sup>2</sup>/g).

Fig. 7 shows the HRSEM morphology of all the synthesized catalysts. BiOBr flakes with thickness range from 40 to 65 nm are



**Fig. 7.** SEM images of (a) BiOBr, (b) 5-ST/BB, (c) 10-ST/BB, (d) 30-ST/BB, (e) 50-ST/BB, (f) 70-ST/BB and (g) SrTiO<sub>3</sub>.

stacked and intercrossed to form flower like structure [64]. Cubes of SrTiO<sub>3</sub> with sizes varying between 8 nm and 50 nm are seen in Fig. 7b [65,66]. When BiOBr was heterojunctioned with SrTiO<sub>3</sub> the flower shape was disbanded and the flakes were seamed with cubes. Strontium titanate cubes were intercalated and placed on the surface of flower like BiOBr. The TEM images of the most active catalyst 10-ST/BB are shown in Fig. 8. Fig. 8a and b show the HRTEM images of the 10-ST/BB which clearly demonstrate the combined structures of both SrTiO<sub>3</sub> and BiOBr. In the HRTEM images of 10-ST/BB catalyst one can see SrTiO<sub>3</sub> heterojunctioned with BiOBr. As indicated in the figure the flower like BiOBr and crystalline SrTiO<sub>3</sub> cubes are present in the composite [65,67]. The proportion of elements (O, Ti, Br, Sr and Bi) present in the catalyst was determined by EDAX and confirmed by elemental mapping as shown in Fig. 8d.

#### 3.1.4. Charge separation efficiency of the catalysts

From photoluminescence spectra, one can understand the rate of electron-hole pair recombination in the photocatalyst. Although PL emission intensity is dependent on the radiation on the surface and the structural defects of photocatalyst, the higher PL intensity, generally indicates the higher recombination of electron hole pair and lower photocatalytic activity [53]. Fig. 9a shows the photoluminescence spectra of BiOBr, SrTiO<sub>3</sub> and 10-ST/BB. Since SrTiO<sub>3</sub> has been calcined at 650 °C, a highly crystalline, ordered cubic structure with less extrinsic defects has been formed. Therefore the PL intensity of SrTiO<sub>3</sub> is very low [68,69]. When the PL intensity of BiOBr and

other composite catalysts are compared, composite catalyst show much less intensive peaks than BiOBr. Not much difference in PL intensity was observed among the composite catalysts. This shows that the recombination rate in the composite catalysts is smaller than BiOBr. The highest PL intensity of BiOBr at 441 nm is due to the presence of more defects in the amorphous structure [70,71]. The PL studies show that the optical property is not the only reason for higher catalytic activity but one should consider the synthesis parameters such as calcination temperature etc [32].

In the photocatalysis reaction, electron transfer resistance and separation efficiency of photogenerated electrons and holes are the most important factors and hence EIS of BiOBr, SrTiO<sub>3</sub> and the most active catalyst (10-ST/BB) were recorded [72]. Their Nyquist plots are shown in Fig. 9b. Electron transfer resistance can be easily understood by the EIS spectra of the different catalysts. In general, lower the radius of the arc, lower the electron transfer resistance [61,73,74]. Among the catalysts, 10-ST/BB composite catalyst showed a better and lower curve than the other catalysts indicating the lowest electron transfer resistance. Such a small difference in impedance also has been reported by Cui et al. [52]. This lowest electron transfer resistance may be ascribed to the introduction of SrTiO<sub>3</sub> nanocubes into the flower like flakes of BiOBr forming an intimate contact with each other which results in higher photocatalytic activity [61,75–77].

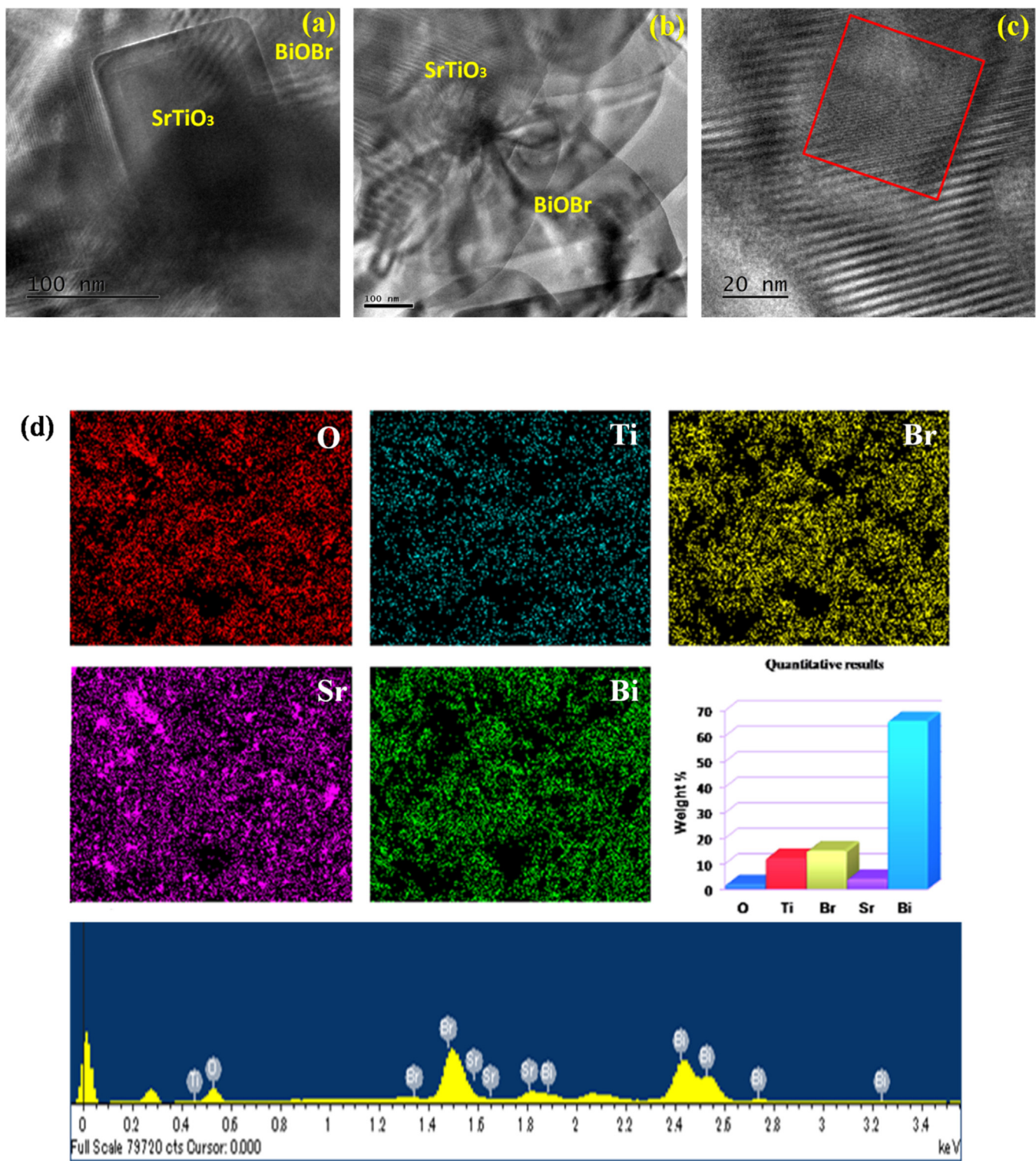


**Fig. 8.** (a–b) TEM, (c) HRTEM and (d) Elemental mapping with EDAX of 10-ST/BB catalyst.

### 3.2. Photocatalytic decolourization studies – optimization of reaction parameters

The percentage decolourization of dyes is dependent on reaction parameters such as initial concentration, pH of dye solution and catalyst weight. Preliminary studies in the decolourization of three different dyes over the synthesized bare catalysts suggested that

BiOBr is a better catalyst than SrTiO<sub>3</sub> and hence all the optimization studies were carried out using BiOBr catalyst.

#### 3.2.1. Effect of initial dye concentration on decolourization

100 ml aliquots of different concentration (10, 30, 50, 70, 90 and 110 ppm) of the three dyes (reactive blue 198, reactive black 5 and reactive yellow 145) along with 50 mg BiOBr catalyst were taken in the quartz vessels of visible light photocatalytic reactor. The pho-

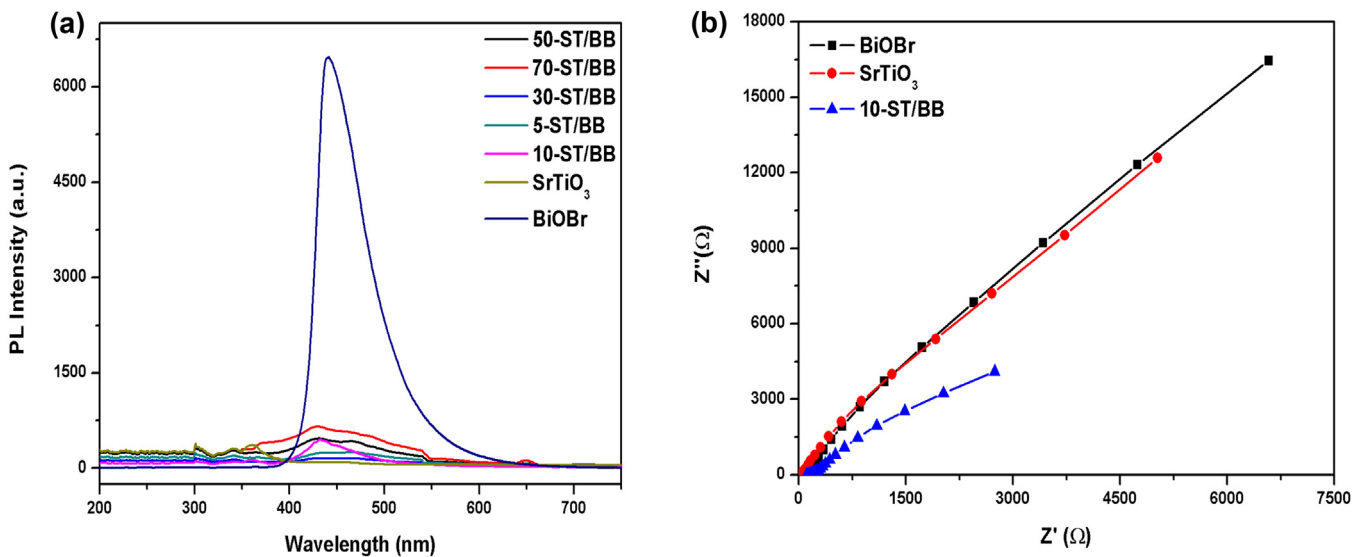


**Fig. 9.** (a) Photoluminescence and (b) electronic impedance spectra of SrTiO<sub>3</sub>, BiOBr and 10-ST/BB catalysts.

**Table 3**

Apparent rate constant and R<sup>2</sup> values in the degradation of reactive dyes.

Catalyst	Reactive blue 198 K <sub>app</sub> (min <sup>-1</sup> ) R <sup>2</sup>	Reactive black 5 K <sub>app</sub> (min <sup>-1</sup> ) R <sup>2</sup>	Reactive yellow 145 K <sub>app</sub> (min <sup>-1</sup> ) R <sup>2</sup>	
Blank	0.00027	0.93080	0.00112	0.98611
SrTiO <sub>3</sub>	0.00251	0.95019	0.00152	0.97844
5-ST/BB	0.04015	0.98073	0.01956	0.95811
10-ST/BB	0.09710	0.96143	0.05234	0.96103
30-ST/BB	0.09703	0.99552	0.03003	0.94444
50-ST/BB	0.02221	0.90972	0.01869	0.98270
70-ST/BB	0.01365	0.90597	0.01209	0.98123
BiOBr	0.02070	0.97190	0.01657	0.98503

tocatalytic decolourization of different dyes at their natural pH was investigated. The effect of initial concentration of various dyes on decolourization was found out and shown in Fig. 10(a–c). For all the dyes the percentage decolourization decreased with increase in the concentration. When the concentration of dyes was increased from 10 ppm to 50 ppm, a large variation in percentage decolourization was observed i.e. from 83.9% to 45% and beyond 50 ppm there was not much difference in the decolourization (Fig. 10g). At lower concentration of the dye, number of active sites on the surface of the catalysts were more than the number of dye molecules to be degraded and hence the decolourization was found to be very high at lower concentration and when the concentration increases further there comes a saturation point and beyond that excess dye is present in the reaction system. The another reason for lower decolourization at higher concentration is “shadow effect” i.e. the dye molecules does not allow enough light to penetrate through it to reach the catalyst surface. Hence 50 ppm was found to be the optimum initial concentration.

### 3.2.2. Effect of catalyst dosage

The effect of weight of catalyst on percentage decolourization was studied by varying the weight of the catalyst from 25 to 150 mg (Fig. 10d). The optimized initial concentration of 50 ppm was taken and the decolourization was carried out at the dyes natural pH. It has been observed from the figure that with increase in the weight of the catalyst, the percentage decolourization increased. There was a substantial increase upto 100 mg of the catalysts and thereafter the percentage decolourization levelled off for all the three dyes. Increase in the weight of catalyst augments generation of more number of electron and hole pairs and hence leads to the formation of more oxidising radicals. However, further increase in the catalyst

weight diminishes the light penetration to the catalyst surface. As a result 100 mg catalyst was taken as optimum catalyst weight for further reactions.

### 3.2.3. Effect of pH of the dye solution

pH is another factor which plays an important role in the photodecolourization of dyes. It explains the charges on the surface of the photocatalyst. It also influences the kinetic studies of organic compounds degradation. The effect of pH on percentage decolourization is shown in Fig. 10i. The pH was varied from 3 to 13 and the percentage decolourization of all the three dyes at the optimized concentration of 50 ppm and the optimized catalyst weight of 100 mg was found out. All the dyes except reactive yellow 145 showed very high decolourization at pH = 7. As there was not much difference in percentage decolourization at pH between 3 and 7 for reactive yellow 145, the pH has been optimized at 7 for further studies. The lower percentage decolourization at higher pH values may be due to electrostatic repulsion between OH<sup>-</sup> ions and the negatively charged BiOBr surface [78–82].

## 3.3. Photocatalytic activity of ST/BB heterojunction catalysts

### 3.3.1. Photocatalytic efficiency of catalysts under visible irradiation

The catalytic activities of all the synthesized catalysts were evaluated towards the decolourization of three different reactive dyes under visible light irradiation and the results are shown in Fig. 11. The figure suggests that there was no decolourization without the catalyst. Petite adsorption of dyes over the catalysts decreased the concentration of dyes slightly in the samples withdrawn after equilibrium of dye solution with catalysts in the absence of light.

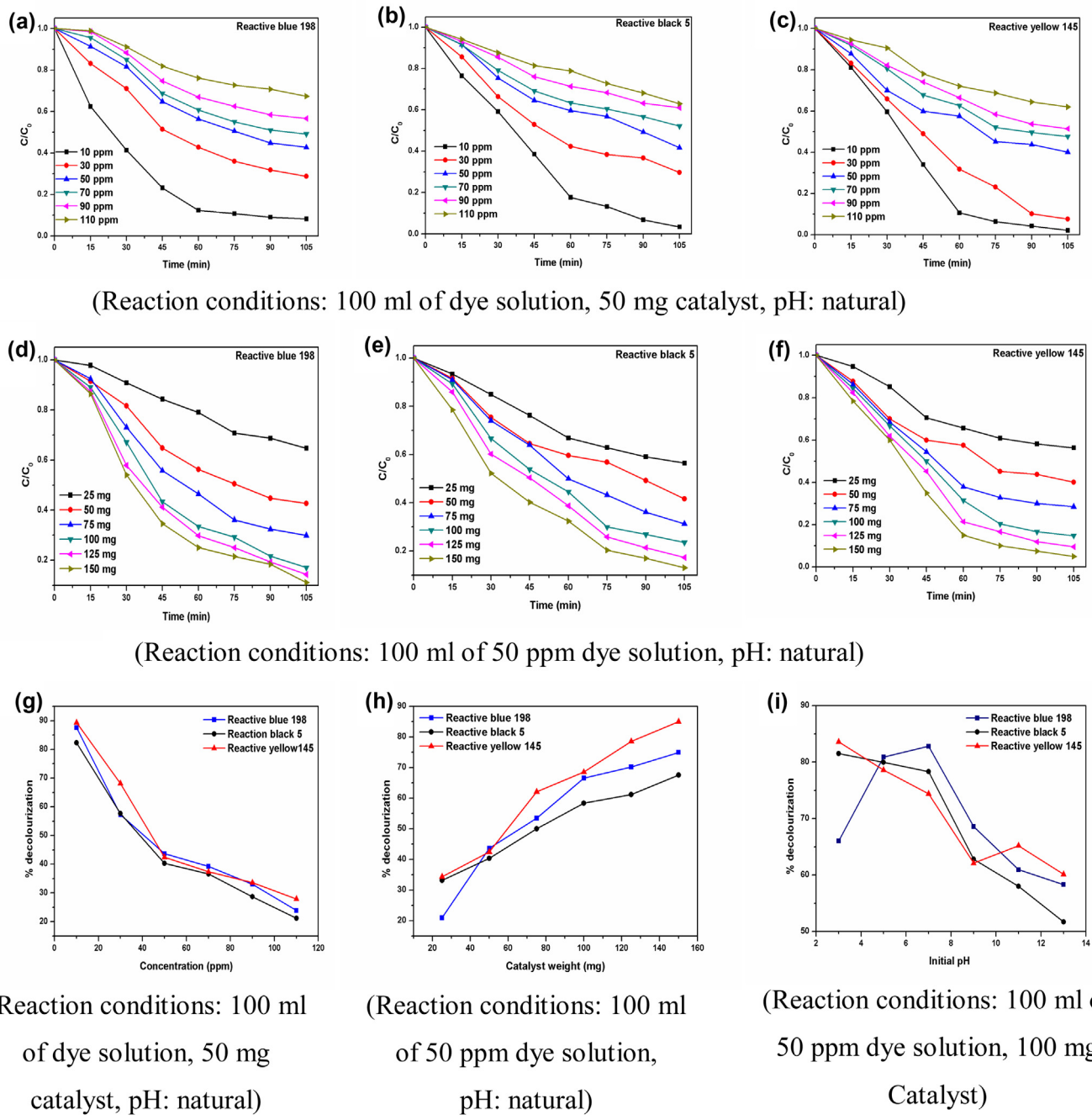


**Fig. 10.** Optimization of various reaction parameters in the decolourization of different dyes.

During photolysis (i.e. without the catalyst) no significant reduction in the concentration of dyes was observed. However during photocatalytic reaction all the three dyes were decolourized to different extents at a much faster rate. Among the catalysts  $\text{SrTiO}_3$  showed the least activity. All the heterojunction catalysts except 70-ST/BB showed higher catalytic activity than both bare  $\text{SrTiO}_3$  and bare  $\text{BiOBr}$  catalysts. Among the ST/BB catalysts, 10-ST/BB showed the highest activity towards the decolourization of all the three dyes. This heterojunction catalyst decolourized almost 100% of reactive blue 198 in 30 min, reactive black 5 in 90 min and reactive yellow 145 in 60 min. The photocatalytic efficiency of all the catalysts towards the decolourization of the three reactive dyes

was found to be in the order 10-ST/BB > 30-ST/BB > 5-ST/BB > 50-ST/BB >  $\text{BiOBr}$  > 70-ST/BB >  $\text{SrTiO}_3$ .

### 3.3.2. Kinetic studies of the photocatalytic reaction

From the following well established and modified Langmuir-Hinshelwood expression  $k_{\text{app.}} = -\ln(C/C_0)/t$ , the apparent rate constant values ( $k_{\text{app.}}$ ) were calculated from the slope of linear regression obtained from the plot of  $-\ln(C/C_0)$  vs time (Fig. 12) [83,84]. Where,  $C$  is the concentration of dye solution at time  $t$ . The straight lines indicate that the decolourization followed pseudo first order kinetics with respect to dye concentration [85]. The apparent rate constant and the correlation coefficient ( $R^2$ ) of the all the catalysts in the decolourization of three dyes are listed in

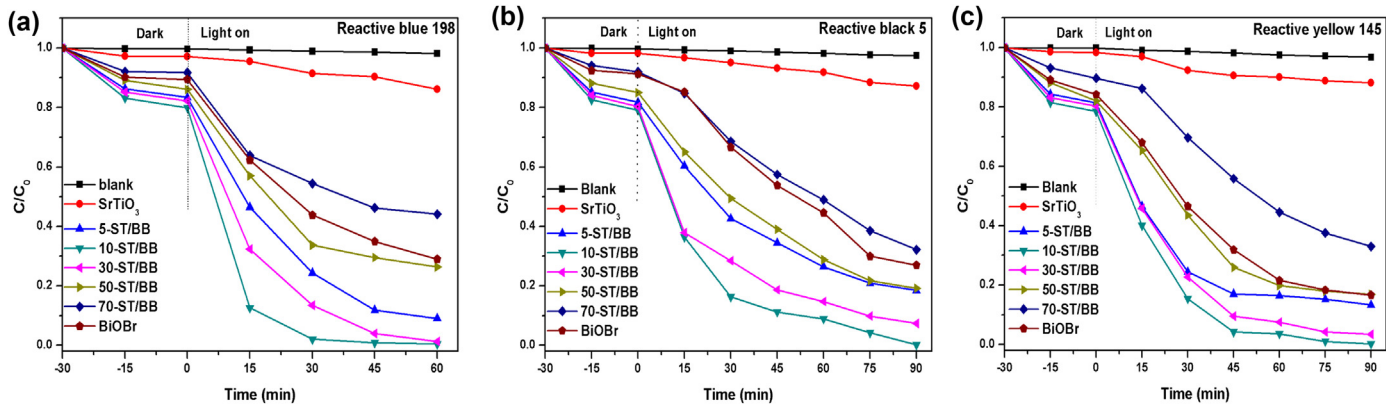


Fig. 11. Photodecolourization of different dyes over synthesized catalysts.

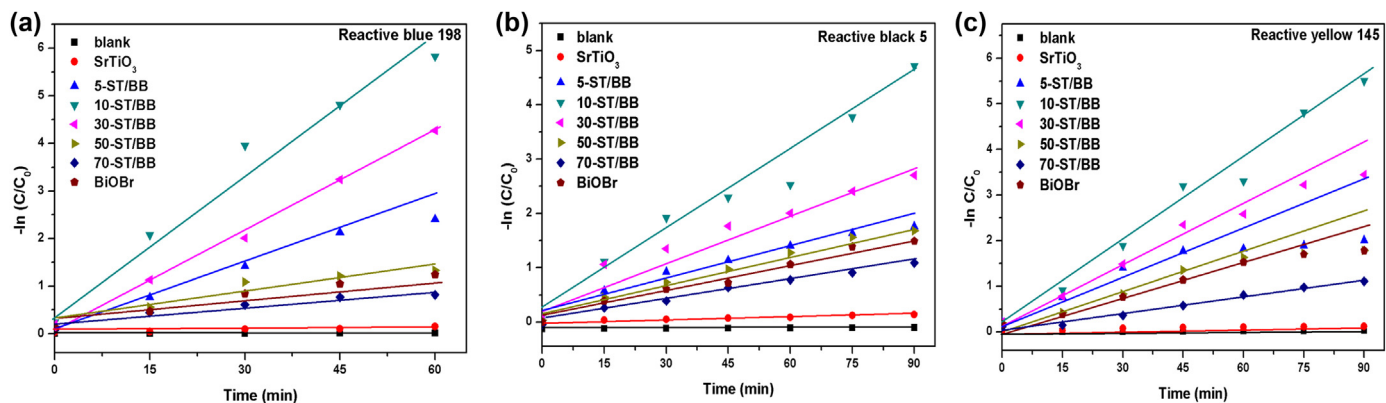


Fig. 12. Kinetic plots in the decolourization of dyes over different catalysts.

**Table 3.** The rate constant value of 10-ST/BB was found to be the highest for the decolourization of all the three reactive dyes. This again indicates that 10-ST/BB is the most active catalyst among the different catalysts synthesized in the present study.

### 3.3.3. HPLC studies on photocatalyzed dyes

In order to check whether the photocatalytic reaction on dyes has resulted in only decolourization or also in degradation, the photocatalyzed dyes were subjected to high performance liquid chromatographic analysis. Since reactive black 5 and reactive yellow 145 showed maximum decolourization at 90 min and reactive blue 198 at 60 min, the dye samples collected at these times were analyzed and compared with samples taken at different times (Fig. 13). The representative chromatogram shown in the figure confirms that all the dyes are degraded significantly. Reactive blue 198, reactive black 5 and reactive yellow 145 got eluted from the chromatographic column at 3.66, 3.62 and 4.8 min respectively. The intensity of these peaks reduced drastically and reached almost zero in all the cases. The formation of some other intermediates in the degradation of reactive blue 198 and reactive yellow 145 is also noted. However during extended period of the photocatalytic reaction the intermediates also degrade and mineralize into some organic salts such as acetates, formates, etc.,  $\text{CO}_2$ , water and salts (Fig. 14). Both COD and TOC values were found to be lower than percentage decolourization values for all the three dyes. These values suggest that dyes which are decolourized are not completely degraded. Dyes decolourize when the chromophoric group is destroyed and the decolourized dyes may degrade into various organic salts such as acetates, formates, etc.,  $\text{CO}_2$ , water and salts.

### 3.3.4. Stability and reusability properties of 10-ST/BB catalyst

To know the photostability of the most active catalyst (10-ST/BB), recyclization was performed towards the decolourization of all the three dyes in presence of visible light (500 W tungsten lamp). The catalyst was centrifuged after the reaction washed, dried and used for next cycle. Four cycles were performed in the decolourization of all the three dyes and the results are displayed in Fig. 15(a–c). The results indicates that the reactive blue 198 has been decolourized from 99.7% to 95%, reactive black 5 from 99.5% to 91.9% and reactive yellow 145 from 99.6% to 98.1% after four cycles. A small variation in the percentage decolourization of different dyes due to loss of catalyst during filtration proves that 10-ST/BB is the most stable catalyst. The SEM image of 10-ST/BB which has been used four times shown in Fig. 16 also confirms the intact nature of the catalyst. The used catalyst had the same flower like morphology containing few cubes.

### 3.4. Efficiency of 10-ST/BB catalyst on dye degradation under solar irradiation

The photocatalytic activity of the preeminent catalyst 10-ST/BB towards the decolourization of reactive blue 198, reactive black 5 and reactive yellow 145 dyes in presence of sunlight is shown in Fig. 17(a–d). These figures clearly indicate that all the three dyes are completely decolourised at a much faster time under solar irradiation than under visible irradiation. All the dyes were decolourized within 20 min of the start of the reaction. Since solar light is the mixture of large amount of visible and certain amount of ultraviolet radiations the decolourization has been faster when compared to visible radiation.

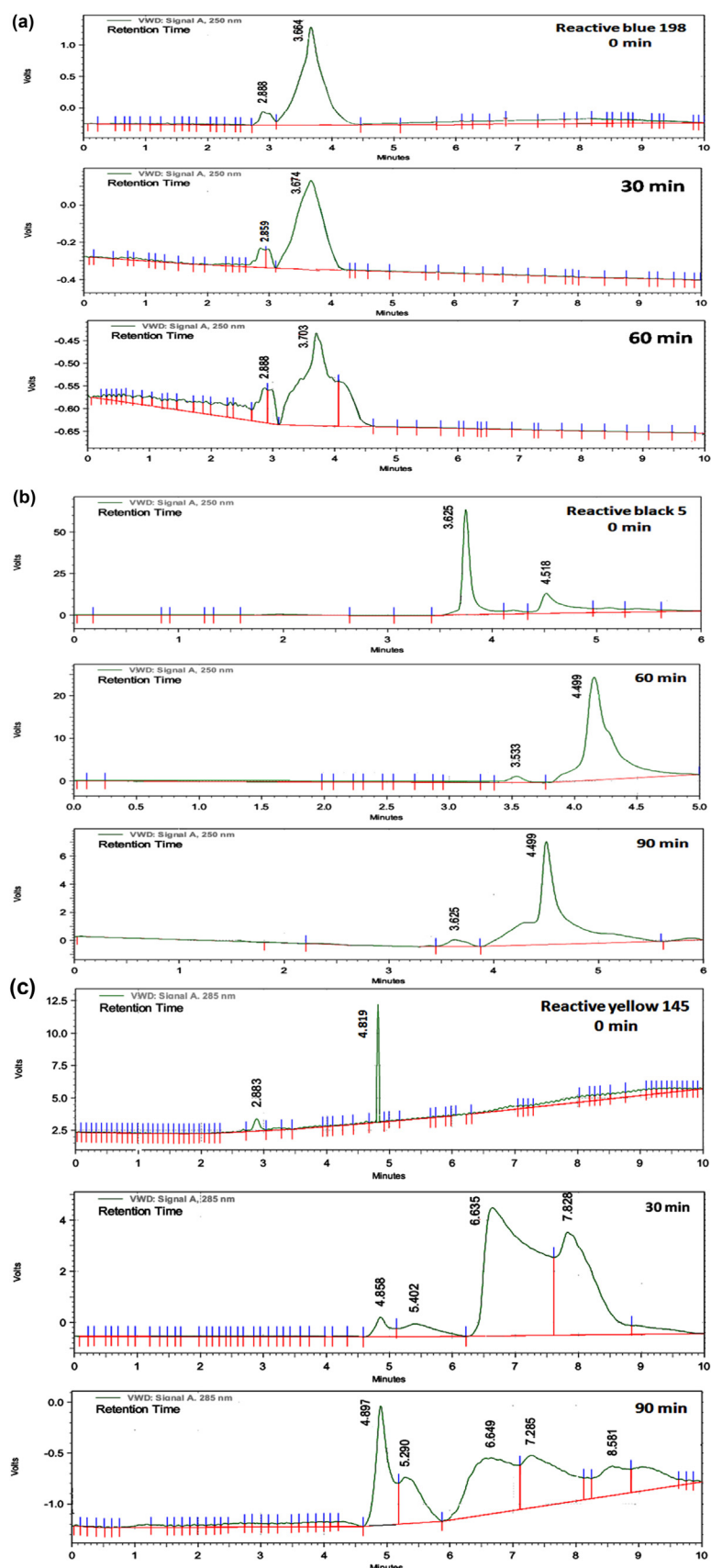


**Fig. 13.** High performance liquid chromatograms of different dyes.

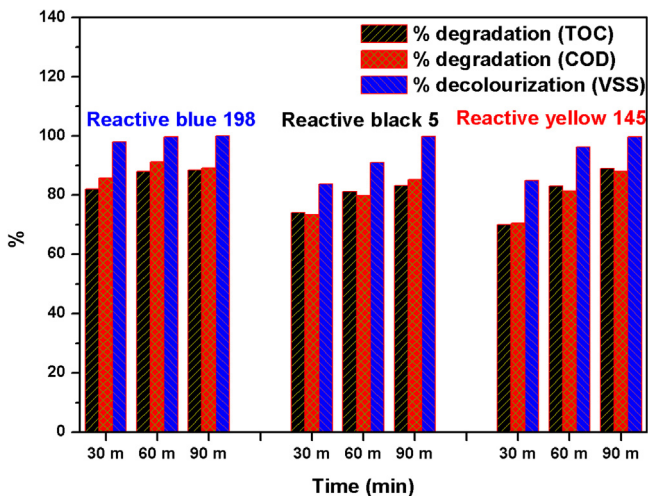


Fig. 14. Percentage degradation vs decolourization of three dyes photocatalysed by 10-ST/BB.

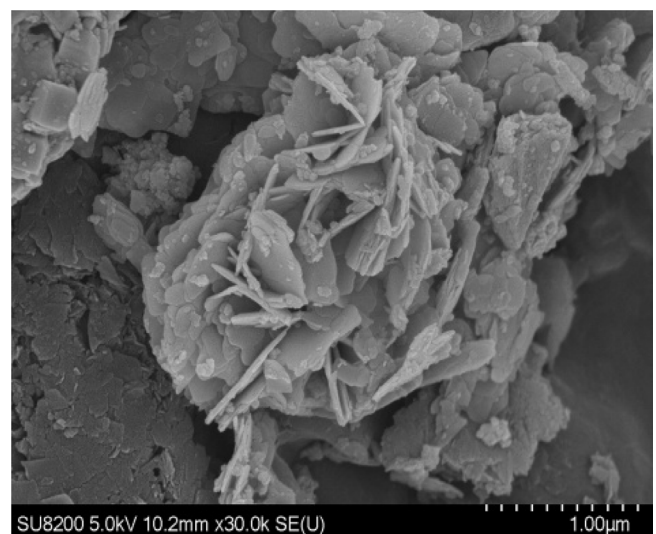


Fig. 16. SEM image of used 10-ST/BB catalyst.

### 3.5. Possible mechanism for the enhanced photocatalytic activity $\text{SrTiO}_3/\text{BiOBr}$ catalyst

The enhanced photocatalytic activity of  $\text{SrTiO}_3/\text{BiOBr}$  heterojunction catalyst is due to the synergistic effect causing effective separation of photo generated holes and electrons. The possible mechanism of the photocatalytic reaction is illustrated in **Scheme 1**.  $\text{BiOBr}$  with 2.8 eV bandgap is highly visible-active whereas  $\text{SrTiO}_3$  with bandgap of 3.22 eV is more active in the ultraviolet region and less active in the visible region. CB of  $\text{BiOBr}$  (0.22 eV) is more positive than  $\text{O}_2/\text{O}_2^-$  (-0.046 eV) whereas the reduction of  $\text{Bi}^{4+}$  to  $\text{Bi}^{3+}$  (1.59 eV) is more negative than  $\text{OH}^-/\text{OH}$  (1.99 eV). On the other hand the VB of  $\text{SrTiO}_3$  (2.51 eV) is more negative than the VB of  $\text{BiOBr}$  (3.12 eV) and CB of  $\text{SrTiO}_3$  is more negative (-0.71 eV) than CB of  $\text{BiOBr}$  (0.22 eV) [44,86]. Therefore in the heterojunction catalyst Fermi level alignments occur and due to this when light shines on heterojunction catalyst the holes from  $\text{BiOBr}$  move from VB of  $\text{BiOBr}$  to the VB of  $\text{SrTiO}_3$  (Valence Band Maximum) and the holes in  $\text{SrTiO}_3$  degrade the dye molecules into  $\text{CO}_2$ , water and mineral salts. At the same time the electrons from the CB of  $\text{SrTiO}_3$  move to the conduction band of  $\text{BiOBr}$  (Conduction Band Minimum). These electrons reduce the oxygen molecule and generate  $\text{O}_2/\text{O}_2^-$  which in term photo mineralize the dye molecules.

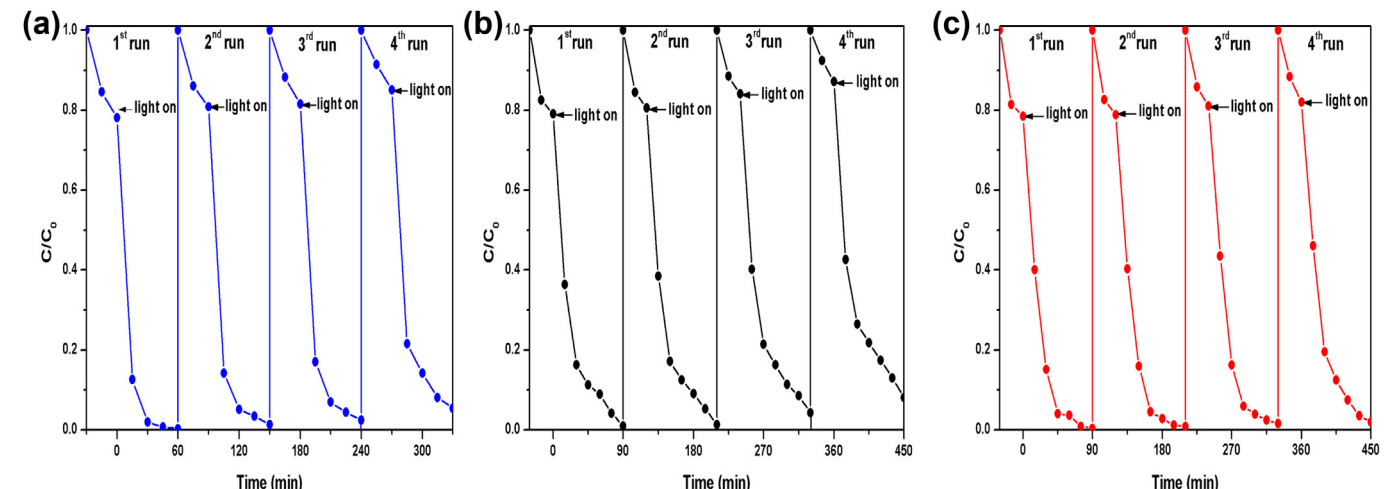


Fig. 15. Recyclability test of 10-ST/BB catalyst in the decolourization of (a) Reactive blue 198, (b) Reactive black 5 and (c) Reactive yellow 145.

### 4. Conclusion

Various weight percentages of  $\text{SrTiO}_3/\text{BiOBr}$  heterojunction catalysts were successfully synthesized by one step precipitation method. XRD, XPS, SEM and TEM images confirmed the formation of heterojunction between  $\text{BiOBr}$  and  $\text{SrTiO}_3$  catalysts. The PL studies indicate that the higher catalytic activity is due to its optical properties but may also be due to the reaction parameters such as calcination temperature etc. EIS of 10-ST/BB composite catalyst confirm lower electron transfer resistance which is attributed to the existence of intimate and intact mixture of  $\text{SrTiO}_3$  and  $\text{BiOBr}$ . The higher activity of composite catalysts than  $\text{BiOBr}$  is ascribed to lower recombination rate and lower electron transfer resistance. HPLC, TOC and COD studies confirm that the photocatalytic reaction not only decolourize the chromophoric groups present in the dyes but also degrade the dyes forming acetate, formate,  $\text{CO}_2$ , water and mineral salts.

### Acknowledgements

The financial support by INSPIRE programme, Department of Science and Technology, New Delhi, India is gratefully acknowl-

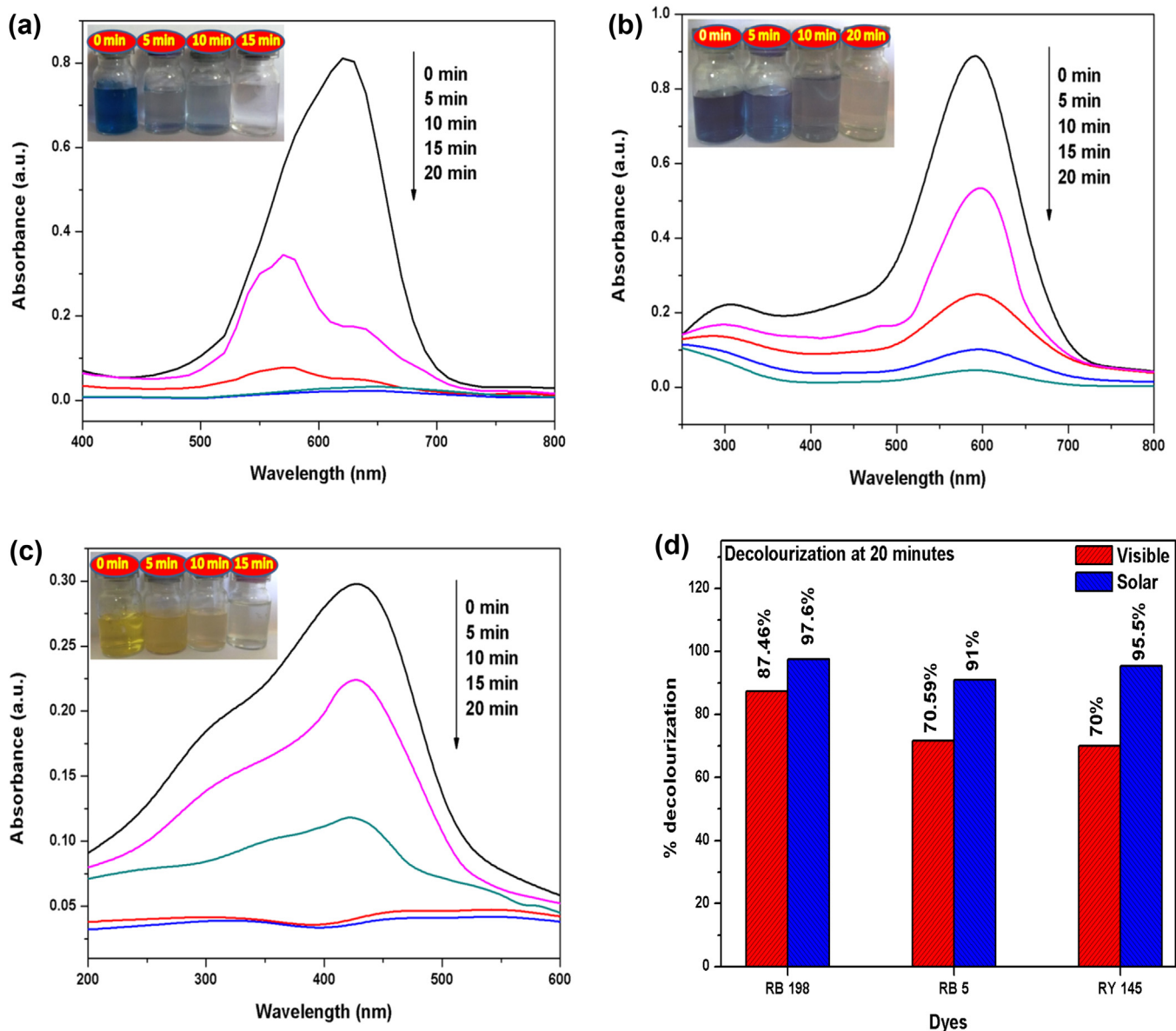
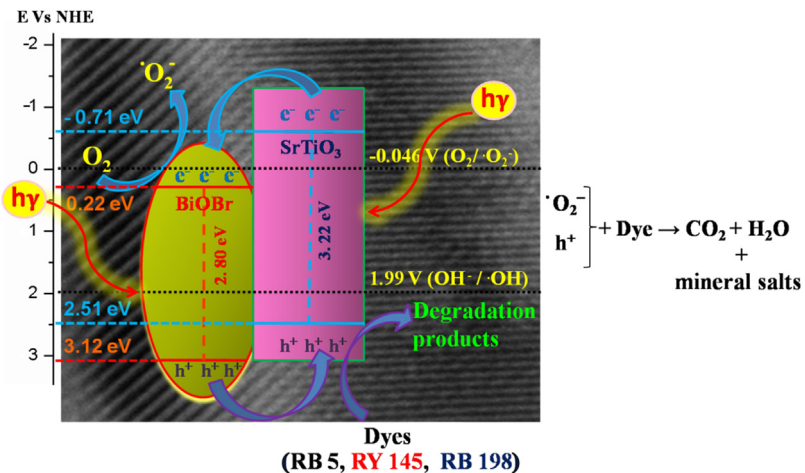


**Fig. 17.** UV visible absorption spectra of (a) Reactive blue 198, (b) Reactive black 5 and (c) Reactive yellow 145 dyes catalyzed by using 10-ST/BB catalyst in the presence of solar irradiation and (d) Percentage decolourization values of dyes in presence of visible and solar irradiations.



**Scheme 1.** Possible photocatalytic mechanism in 10-ST/BB catalyst for dye degradation.

edged. XPS, SEM and TEM studies made at Dr. Hideki Abe's laboratory, NIMS, Tsukuba, Japan is acknowledged.

## References

- [1] A. Houas, H. Lachheb, M. Ksibi, E. Elaloui, C. Guillard, J.M. Herrmann, *Appl. Catal. B. Environ.* 31 (2001) 145–157.
- [2] H. Park, W. Choi, J. Photochem. Photobiol. A 159 (2003) 241–247.
- [3] I.A. Alaton, I.A. Balcioglu, D.W. Bahnemann, *Water Res.* 36 (2002) 1143–1154.
- [4] U. Pagga, D. Brown, *Chemosphere* 15 (1986) 145–491.
- [5] R. Kant, *Nat. Sci.* 4 (2012) 22–26.
- [6] N. Mathur, P. Bathnagar, P. Nagar, M.K. Bijiarnia, *Ecotoxicol. Environ. Saf.* 61 (2005) 105–113.
- [7] O.J. Hao, H. Kim, P.C. Chaing, *Crit. Rev. Environ. Sci. Technol.* 30 (2000) 449–505.
- [8] A.J. De Roos, R.M. Ray, D.L. Gao, K.J. Wernli, E.D. Fitzgibbons, F. Zinding, G. Astrakianakis, D.B. Thoma, H. Checkoway, *Cancer Causes Control* 16 (2005) 1177–1188.
- [9] A. Birhanli, M. Ozmen, *Drug Chem. Toxicol.* 28 (2005) 51–65.
- [10] E.E. Dogan, E. Yesilada, L. Ozata, S. Yologlu, *Drug Chem. Toxicol.* 28 (2005) 289–301.
- [11] I.K. Konstantinou, T.A. Albanis, *Appl. Catal. B. Environ.* 49 (2004) 1–14.
- [12] S. Chiron, A. Fernández-Alba, A. Rodriguez, E.C. Calvo, *Wat. Res.* 34 (2000) 366–377.
- [13] H.D. Burrows, M. Canle, J.A. Santaballa, S. Steenken, *J. Photochem. Photobiol. B: Biol.* 67 (2002) 71–108.
- [14] P. Pekakis, N.P. Xekoukoulotakis, D. Mantzavinos, *Water Res.* 40 (2006) 1276–1286.
- [15] S.F. Kang, C.H. Liao, S.T. Po, *Chemosphere* 41 (2000) 1287–1294.
- [16] Navneet Kaur, Satwant Kaur Shahi, Vasundhara Singh, *Photochem. Photobiol. Sci.* 14 (2015) 2024–2034.
- [17] S.N. Phattalung, S. Limpijumnong, J. Yu, *Appl. Catal. B. Environ.* 200 (2017) 1–9.
- [18] J.K. Zhou, L. Lv, J.Q. Yu, H.L. Li, P.Z. Guo, H. Sun, X.S. Zhao, *J. Phys. Chem. C* 112 (2008) 5316–5321.
- [19] E.J. Wang, T. He, L.S. Zhao, Y.M. Chen, Y.A. Cao, *J. Mater. Chem.* 21 (2011) 144–150.
- [20] M. Ni, M.K.H. Leung, D.Y.C. Leung, K. Sumathy, *Renew. Sustain. Energy Rev.* 11 (2007) 401–425.
- [21] R. Vaithianathan, K. Kathiravan, J. Amala Infant Joice, K. Thamaraiselvi, T. Sivakumar, *J. Nanosci. Nanotechnol.* 16 (2016) 9980–9986.
- [22] A. Brindha, K. Kathiravan, T. Sivakumar, *J. Ind. Eng. Chem.* 36 (2016) 184–193.
- [23] J. Amala Infant Joice, T. Sivakumar, *RSC Adv.* 5 (2015) 9792–9805.
- [24] J. Amala Infant Joice, R. Ramakrishnan, S. Kalaivani, T. Sivakumar, *Appl. Surf. Sci.* 258 (2011) 2515–2521.
- [25] J. Amala Infant Joice, S. Kalaivani, S. Divya, E. Rajesh Kannan, T. Sivakumar, *Trans. Ind. Ceram. Soc.* 70 (2011) 109–114.
- [26] A. Valentine Rupa, R. Vaithianathan, T. Sivakumar, *Water Sci. Technol.* 64 (2011) 1040–1045.
- [27] T. Cao, Y. Li, C. Wang, C. Shao, Y. Liu, *Langmuir* 27 (2011) 2946–2952.
- [28] F. Silly, M.R. Castell, *J. Phys. Chem. B* 109 (2005) 12316–12319.
- [29] R. Konta, T. Ishii, H. Kato, A. Kudo, *J. Phys. Chem. B* 108 (2004) 8992–8995.
- [30] A.D. Paola, E.G. Lopez, G. Marci, L. Palmisan, *J. Hazard. Mater.* 211 (2010) 3–29.
- [31] J. Li, Y. Yu, L. Zhang, *Nanoscale* 6 (2014) 8473–8488.
- [32] L. Ruan, J. Liu, Q. Zhou, J. Hu, G. Xu, X. Shu, Y. Wu, *New J. Chem.* 38 (2014) 3022–3028.
- [33] L. Chen, J. He, Q. Yuan, Y. Liu, C.T. Au, S.F. Yin, *J. Mater. Chem. A* 3 (2015) 1096–1102.
- [34] Q. Yuan, L. Chen, M. Xiong, J. He, S.L. Luo, C.T. Au, S.F. Yin, *J. Chem. Eng.* 255 (2014) 394–402.
- [35] X. Zhang, Z.H. Ai, F.L. Jia, L.Z. Zhang, *J. Phys. Chem. C* 112 (2008) 747–753.
- [36] F. Duan, X. Wang, T. Tan, M. Chen, *Phys. Chem. Chem. Phys.* 18 (2016) 6113–6121.
- [37] J. Xia, S. Yin, H. Li, H. Xu, L. Xu, Y. Xu, *Dalton Trans.* 40 (2011) 5249–5258.
- [38] J.L. Wang, Y. Yu, L.Z. Zhang, *Appl. Catal. B* 136 (2013) 112–121.
- [39] S. Vadivel, P. Keerthi, M. Vanitha, A. Muthukrishnaraj, N. Balasubramanian, *Mater. Lett.* 128 (2014) 287–290.
- [40] J. Zhang, L. Zhang, J. Lv, S. Zhou, H. Chen, Y. Zhao, X. Wang, *Appl. Surf. Sci.* 90 (2014) 135–140.
- [41] T.M. Thi, L.V. Tinh, B.H. Van, P.V. Ben, V. Trung, *J. Nanomater.* 2012 (2012) 528047–528048.
- [42] V.M. Longo, A.T. de Figueiredo, S. de Lázaro, M.F. Gurgel, M.G. Costa, *J. Appl. Phys.* 104 (2008), 023515–11.
- [43] A. Jia, Z. Su, L.L. Lou, S. Liu, *Solid State Sci.* 12 (2010) 1140–1145.
- [44] L. Ye, J. Liua, Z. Jiang, T. Penga, L. Zan, *Appl. Catal. B Environ.* 142 (2013) 1–7.
- [45] L. Chen, S. Zhang, L. Wang, D. Xue, S. Yin, *J. Cryst. Growth* 311 (2009) 746–748.
- [46] D. Wu, B. Wang, W. Wang, T. An, G. Li, T.W. Ng, H.Y. Yip, C. Xiong, H.K. Lee, P.K. Wong, *J. Mater. Chem. A* 3 (2015) 15148–15155.
- [47] P. Jing, W. Lan, Q. Su, E. Xie, *Belistein J. Nanotechnol.* 6 (2015) 1281–1286.
- [48] L. Chen, R. Huang, M. Xiong, Q. Yuan, J. He, J. Jia, M.Y. Yao, S.L. Luo, C.T. Au, S.F. Yin, *Inorg. Chem.* 52 (2013) 11118–11125.
- [49] B. Vincent Crist, *XPS Rev.* 1 (2007) 1–52.
- [50] Y.P. Jiang, X.G. Tang, Y.C. Zhou, Q.X. Liu, *Prog. Nat. Sci.: Mater. Int.* 21 (2011) 198–204.
- [51] F. Puleo, L.F. Liotta, V.L. Parola, D. Banerjee, A. Martorana, A. Longo, *Phys. Chem. Chem. Phys.* 16 (2014) 22677–22686.
- [52] W. Cui, W. An, L. Liu, J. Hu, Y. Liang, *J. Hazard. Mater.* 280 (2014) 417–427.
- [53] S. Azad, M.H. Engelhard, L.Q. Wang, *J. Phys. Chem. B* 109 (2005) 10327–10331.
- [54] P.S. Bagus, E.S. Ilton, C.J. Nelin, *Surf. Sci. Rep.* 68 (2013) 273–304.
- [55] M. Rezvani, L. Farahani, *Mater. Des.* 88 (2015) 252–257.
- [56] Z.S. Liu, B.T. Wu, Y.L. Zhao, J.N. Niu, Y.B. Zhu, *Ceram. Int.* 40 (2014) 5597–5603.
- [57] O. Mehraj, N.A. Mir, B.M. Pizada, S. Sabir, *Appl. Surf. Sci.* 332 (2015) 419–429.
- [58] N.H. Park, F. Dang, C. Wan, W.S. Seo, K. Koumoto, *J. Asian Ceram. Soc.* 1 (2013) 35–40.
- [59] D.S. Bhachu, S.J.A. Moniz, S. Sathasivam, D.O. Scanlon, A. Walsh, S.M. Bawaked, M. Moktar, A.Y. Obaid, I.P. Parkin, J. Tang, C.J. Carmalt, *Chem. Sci.* 7 (2016) 4832–4841.
- [60] M.N. Ha, F.Z. Zhu, Z. Liu, L. Wang, L. Liu, G. Lu, Z. Zhao, *RSC Adv.* 6 (2016) 21111–21118.
- [61] J. Di, J. Xia, Y. Ge, L. Xu, H. Xu, J. Chen, M. He, H. Li, *Dalton Trans.* 43 (2014) 15429–15438.
- [62] Y. Feng, L. Li, J. Li, J. Wang, L. Liu, *J. Hazard. Mater.* 192 (2011) 538–544.
- [63] S. Wu, Q. Dong, J. Wang, Q. Jia, Y. Sun, S. Shan, Y. Wang, *J. Nanomater.* 2015 (2015) 1–6.
- [64] X.X. Wei, H. Cui, S. Guo, L. Zhao, W. Li, *J. Hazard. Mater.* 263 (2013) 650–658.
- [65] F.A. Rabuffetti, H.S. Kim, J.A. Enterkin, Y. Wang, C.H. Lanier, L.D. Marks, K.R. Poeppelmeier, P.C. Stair, *Chem. Mater.* 20 (2008) 5628–5635.
- [66] L. Dong, Q. Luo, K. Cheng, H. Shi, Q. Wang, W. Wang, W.Q. Han, *Sci. Rep.* 4 (2014) 5084–5085.
- [67] X. Zhang, C.Y. Wang, L.W. Wang, G. X. Huang, W.K. Wang, H.Q. Yu, *Sci. Rep.* 6 (2016) 22800–22810.
- [68] M. Zalewska, B.L. Lastowka, A.M. Kionkowski, *J. Non-Cryst. Sol.* 356 (2010) 2070–2075.
- [69] E. Orhan, F.M. Pontes, C.D. Pinheiro, T.M. Boschi, E.R. Leite, P.S. Pizani, A. Beltrand, J. Andres, J.A. Varela, E. Longo, *J. Solid State Chem.* 177 (2004) 3879–3885.
- [70] H. Li, T. Hu, N. Du, R. Zhang, J. Liu, W. Hou, *Appl. Catal. B Environ.* 187 (2016) 342–349.
- [71] W. An, W. Cui, Y. Liang, J. Hu, L. Liu, *Appl. Surf. Sci.* 351 (2015) 1131–1139.
- [72] J. Cao, B. Xu, B. Luo, H. Lin, S. Chen, *Catal. Commun.* 13 (2011) 63–68.
- [73] E. Echeverri, O. Arnache, *J. Phys.* 687 (2016) 012040–012044.
- [74] L. Xu, J. Xia, K. Wang, L. Wang, H. Li, H. Xu, L. Huang, M. He, *Dalton Trans.* 42 (2013) 6468–6477.
- [75] Y. Zhao, T. Yu, X. Tan, C. Xie, S. Wang, *Dalton Trans.* 44 (2015) 20475.
- [76] D. Wu, B. Wang, W. Wang, T. An, G. Li, T.W. Ng, H.Y. Yip, C. Xiong, H.K. Lee, P.K. Wong, *J. Mater. Chem. A* 3 (2015) 15148–15155.
- [77] Q. Du, W. Wang, Y. Wu, G. Zhao, F. Ma, X. Hao, *RSC Adv.* 5 (2015) 31057–31063.
- [78] S. Alahiane, S. Oourzal, M.E. Ouardi, A. Abaamrane, A. Assabbane, *Am. J. Anal. Chem.* 5 (2015) 445–454.
- [79] A. Guedach, S. Brosillon, J. Morvan, E.K. Lhadi, *Appl. Catal. B Environ.* 57 (2005) 55–62.
- [80] W.L. Li, M. Hong, W.S. Lian, Z. Yu, J.M. Ke, L.R. Ping, Z.A. Quing, H.Y. Ping, *J. Nanomater.* 2012 (2012) 619761–619769.
- [81] T.H. Bokhari, M. Kashif, I. Bhatti, M. Zubair, S. Adeel, M. Yousaf, M. Ahmad, M. Iqbal, M. Usman, M. Zuber, A. Mansha, *Asian J. Chem.* 25 (2013) 8668–8672.
- [82] H.A. Ekabi, N. Serpone, *J. Phys. Chem.* 92 (1988) 5731–5738.
- [83] J.B.D. Heredia, J. Torregrosa, J.R. Dominguez, J.A. Peres, *J. Hazard. Mater.* B 83 (2001) 255–264.
- [84] I.K. Konstantinou, T.A. Albanis, *Appl. Catal. B Environ.* 49 (2004) 1–14.
- [85] X. Xiao, R. Hu, S. Tu, C. Zheng, H. Zhong, X. Zuo, J. Nan, *RSC Adv.* 5 (2015) 38373–38381.
- [86] S. Gerhold, M. Riva, Z. Wang, R. Bliehm, M. Wagner, J. Osiecki, K. Schulte, M. Schmid, U. Diedold, *J. Phys. Chem. C* 119 (2015) 20481–20487.